

# Developmental Control of Nuclear Size and Shape by *kugelkern* and *kurzkern*

Annelly Brandt,<sup>1,\*</sup> Fani Papagiannouli,<sup>1</sup>  
Nicole Wagner,<sup>2</sup> Michaela Wilsch-Bräuninger,<sup>3</sup>  
Martina Braun,<sup>4</sup> Eileen E. Furlong,<sup>4</sup> Silke Loserth,<sup>2</sup>  
Christian Wenzl,<sup>1</sup> Fanny Pilot,<sup>5</sup> Nina Vogt,<sup>6</sup>  
Thomas Lecuit,<sup>5</sup> Georg Krohne,<sup>2</sup> and Jörg Großhans<sup>1</sup>

<sup>1</sup>Zentrum für Molekulare Biologie der Universität  
Heidelberg (ZMBH)

Im Neuenheimer Feld 282  
69120 Heidelberg  
Germany

<sup>2</sup>Biozentrum  
Universität Würzburg  
Am Hubland  
97074 Würzburg  
Germany

<sup>3</sup>Max-Planck-Institut für Molekulare Zellbiologie  
und Genetik  
Pfotenhauerstr. 108  
01307 Dresden  
Germany

<sup>4</sup>European Molecular Biology Laboratory  
Meyerhofstrasse 1  
69117 Heidelberg  
Germany

<sup>5</sup>Institut de Biologie du Développement  
de Marseille (IBDM)  
Laboratoire de Génétique et de Physiologie  
du Développement (LGPD)  
Centre National de la Recherche Scientifique  
Unité Mixte de Recherche 6545  
Université de la Méditerranée  
Campus de Luminy, case 907  
13288 Marseille Cedex 09  
France

<sup>6</sup>Max-Planck-Institut für Entwicklungsbiologie  
Spemannstr. 35,  
72076 Tübingen  
Germany

## Summary

**Background:** The shape of a nucleus depends on the nuclear lamina, which is tightly associated with the inner nuclear membrane and on the interaction with the cytoskeleton. However, the mechanism connecting the differentiation state of a cell to the shape changes of its nucleus are not well understood. We investigated this question in early *Drosophila* embryos, where the nuclear shape changes from spherical to ellipsoidal together with a 2.5-fold increase in nuclear length during cellularization.

**Results:** We identified two genes, *kugelkern* and *kurzkern*, required for nuclear elongation. In *kugelkern*- and *kurzkern*-depleted embryos, the nuclei reach only half

the length of the wild-type nuclei at the end of cellularization. The reduced nuclear size affects chromocenter formation as marked by Heterochromatin protein 1 and expression of a specific set of genes, including early zygotic genes. *kugelkern* contains a putative coiled-coil domain in the N-terminal half of the protein, a nuclear localization signal (NLS), and a C-terminal CxxM-motif. The carboxyterminal CxxM motif is required for the targeting of *kugelkern* to the inner nuclear membrane, where it colocalizes with lamins. Depending on the farnesylation motif, expression of *kugelkern* in *Drosophila* embryos or *Xenopus* cells induces overproliferation of nuclear membrane.

**Conclusions:** *kugelkern* is so far the first nuclear protein, except for lamins, that contains a farnesylation site. Our findings suggest that *kugelkern* is a rate-determining factor for nuclear size increase. We propose that association of farnesylated *kugelkern* with the inner nuclear membrane induces expansion of nuclear surface area, allowing nuclear growth.

## Introduction

The morphology of nuclei varies among different developmental stages, tissues, and cell-cycle states. Age-related alterations of nuclear shape, accompanied by loss of peripheral heterochromatin, have been found in *C. elegans* [1] as well as in human cell lines [2]. Abnormalities in nuclear size and shape are frequently observed in malignant tissues [3] or in patients with nuclear envelopathies or certain progeria syndromes [2]. In addition, there is growing evidence that the nuclear lamina has not only structural but also functional impact on the cell by regulating chromatin configuration and influencing gene expression (for review, see [4]). The mechanisms that link the morphology of the nucleus to the developmental program of a cell have not been much analyzed (for review, see [4, 5]).

The shape of a nucleus depends on the nuclear lamina, which is thought to provide mechanical support for the nuclear membrane (NM) and to mediate attachment of interphase chromatin to the nuclear envelope [6, 7]. The lamina consists of a meshwork of nuclear-specific intermediate filaments, the lamin proteins, plus numerous lamin-associated proteins (for review, see [4, 7]). Targeting and association of lamins with the inner membrane is mediated by an evolutionary conserved farnesylation of the CxxM motif at their C termini (for review, see [8, 9]).

In *Drosophila* development, there is a definite event of nuclear shape change, accompanied by massive nuclear growth during the process of cellularization [10]. During cellularization, all cortical nuclei are simultaneously enclosed into membranes, and there is a marked change in the shape of the nuclei from spherical to ellipsoid together with a 2.5-fold increase in nuclear length [11, 12]. The mechanisms and components involved have remained elusive.

\*Correspondence: a.haase@zmbh.uni-heidelberg.de

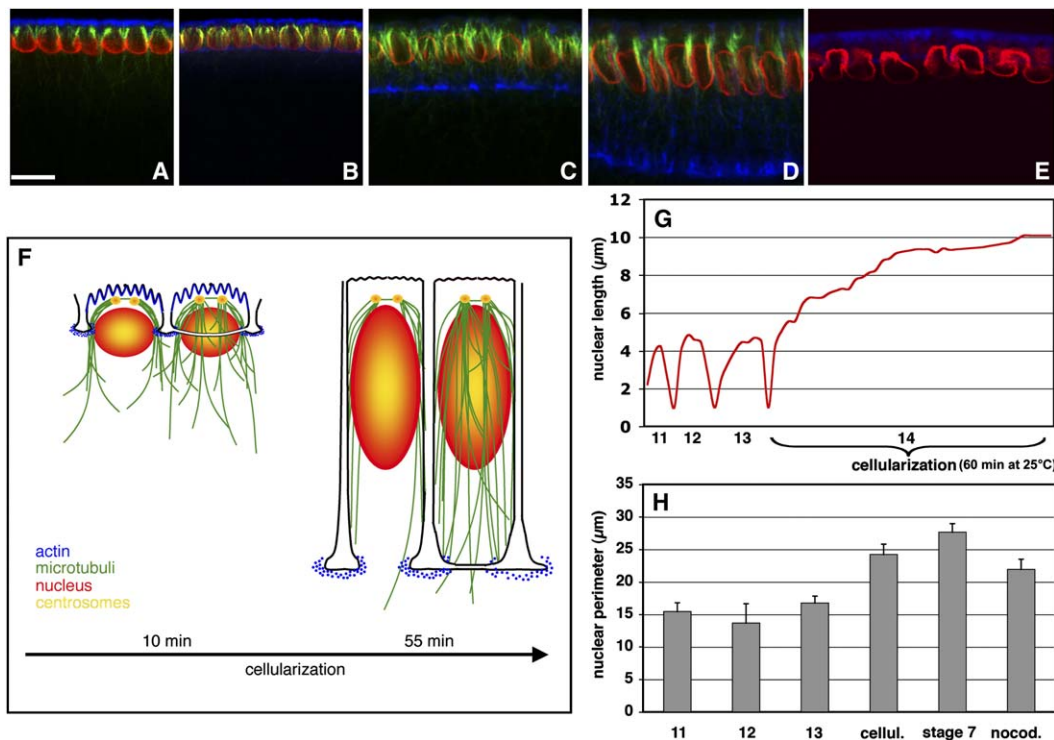


Figure 1. Nuclear Shape Change during Cellularization

(A–E) Wild-type embryos during cellularization stained for Kuk (red), F-actin (blue), and microtubules (green). The scale bar represents 10  $\mu\text{m}$ . (E) Nocodazole-treated embryo; note the absence of microtubuli (green).

(F) Schematic overview of cellularization.

(G) Kinetics of nuclear length (apical-basal axis) during cell cycles 11 to 14.

(H) Perimeter of interphase nuclei in different cell cycles, in gastrulation (stage 7) or in nocodazole-treated embryos.  $n = 30$  for each group, error bars = standard deviation. For untreated (cellul.) versus nocodazole-treated (nocod.) embryos:  $n = 30$ , nondirectional Mann-Whitney test,  $p > 0.05$ ,  $U_A = 580$ ,  $z = -1.91$ . For cycle-13 embryos versus nocodazole-treated embryos:  $n = 30$ , nondirectional Mann-Whitney test,  $p < 0.01$ ,  $U_A = 867$ ,  $z = -6.16$ .

The early syncytial blastoderm is characterized by rapid nuclear division cycles, transcriptional silencing, and a homogeneous appearance of the chromatin. At the transition from syncytial to cellular blastoderm, the cell cycle is paused, the transcription rate increases, and chromatin loses its uniform appearance. This change in chromatin organization is highlighted by the appearance of a conspicuous chromocenter [13]. Strikingly, this reorganization of the chromatin takes place during cycle 14 and coincides with the strong increase of zygotic transcription and nuclear elongation.

## Results

### Nuclear Elongation during Cellularization

During cellularization, the shape of the nuclei changes from spherical to ellipsoidal together with a 2.5-fold increase in nuclear length from approximately 4  $\mu\text{m}$  up to 10  $\mu\text{m}$  (Figures 1A–1D, 1F, and 1G). A rearrangement of the microtubuli-based cytoskeleton accompanies membrane invagination and nuclear shape change [11]. As the nucleus assumes an elongated appearance, microtubules extend in close association with the nucleus, mirroring nuclear growth in both direction and rate [11]. To determine whether the nuclear growth depends on microtubules, we treated staged embryos with the

microtubule (MT) polymerization inhibitor nocodazole. After incubation in nocodazole, the nuclei maintained a rounded, irregular shape although their nuclear surface area increased significantly in size (Figures 1E and 1H). Confirming data from [14], we found that MT function is essential for the shape change of the nuclei from spherical to ellipsoidal but not for the nuclear growth.

### *kugelkern* and *kurzkern* Are Required for Nuclear Elongation

We identified two genes required for the process of nuclear elongation in independent screens for genes involved in blastoderm formation. *kugelkern* (*kuk*) was identified by its early zygotic expression (see Experimental Procedures). In embryos injected with *kuk* dsRNA (designated *kuk* embryos) or from *kuk*-deficient females (Figures S1A and S1B in the Supplemental Data available online), the cortical nuclei are spherical by the end of cellularization (Figure 2A). The nuclei reached only the same length as in previous interphases (4  $\mu\text{m}$ ) as compared to wild-type nuclei that finally reached 10  $\mu\text{m}$  in length (Figure 2B). Nevertheless, the cellularization front invaginated with the same velocity as in wild-type embryos. Microtubules and the actin cytoskeleton seemed to be unaffected (Figure 2A, compare to Figure 1D). We could not find any obvious

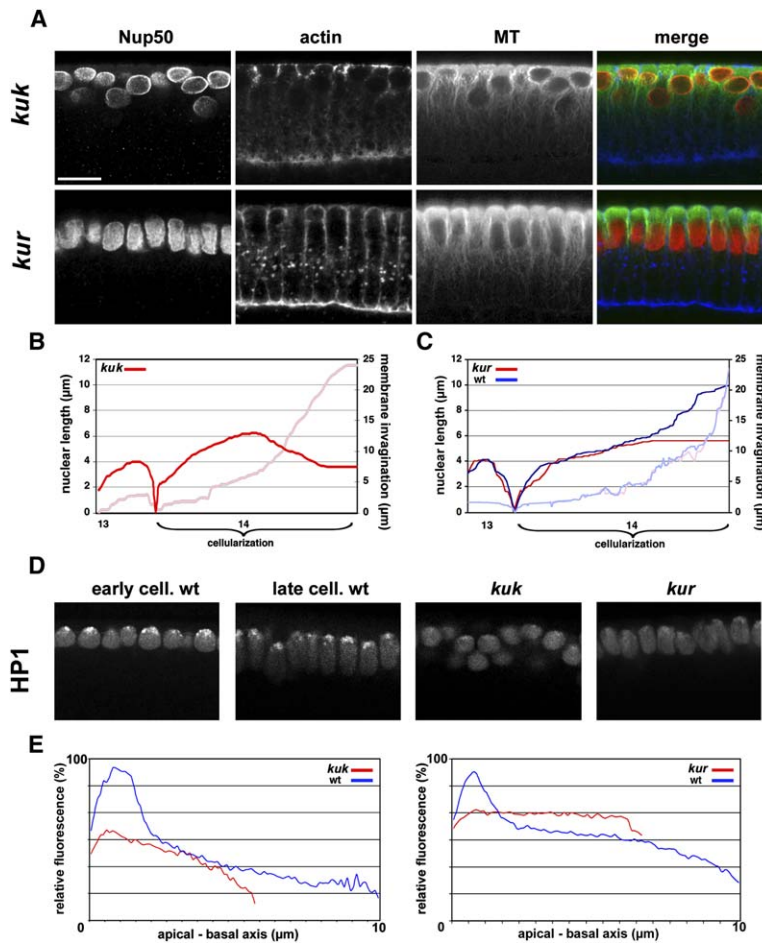


Figure 2. Phenotype of *kuk* and *kur*

(A) *kuk*-RNAi-treated embryo and *kur* embryos at the end of cellularization stained with anti-Nup50 (red), anti- $\alpha$ -Tubulin (green) antibodies, and phalloidin (blue); the scale bar represents 10  $\mu$ m.

(B and C) Kinetics of nuclear length increase and membrane invagination during interphases of cell cycles 13 and 14. Blue line shows nuclear length of wild-type embryos; red line shows *kuk*-deficient embryos (B) or *kur* embryos (C). Length of invaginated membrane is depicted in light blue (wt) and light red (*kuk/kur*).

(D) HP1 staining in wild-type at early and late cellularization or in *kuk* and *kur* embryos late during cellularization.

(E) Relative fluorescence of HP1 staining along the apical-basal axis of the nuclei in wild-type *kuk* (RNAi-treated) and *kur* embryos.

morphological differences between *kuk* and wild-type embryos with regard to the positioning of the nuclei by the end of cellularization (data not shown). *kuk* is not an essential gene, because *kuk*-deficient flies are viable and fertile.

In embryos from *kurzkern* (*kur*) germline clones (*kur* embryos), nuclear elongation was significantly reduced. There was no visible defect prior to cellularization in *kur* embryos when compared to wild-type embryos (Figure 2C). The nuclei of *kur* mutants started to elongate normally in the first half of cellularization. When the invaginating membrane front reached the basal outline of the nuclei, the first retardation compared to the wild-type situation was observed (Figure 2C). Finally, the nuclei accomplished only approximately 60% of the length of wild-type nuclei at the end of cellularization (Figures 2A and 2C). However, in contrast to the wild-type situation, *kur* nuclei did not move basally at the end of cellularization. During gastrulation, *kur* embryos fail to form the cephalic furrow and do not accomplish germband extension; this is comparable to the germband-extension phenotype of *eve* described by [15]. Because this gastrulation phenotype was different from that found in *kuk* embryos, it may represent a second function of *kur* independent of the earlier nuclear-elongation function. In conclusion, we identified two genes, *kuk* and *kur*, that are required for nuclear elongation during cellularization.

### *kuk* and *kur* Affect Chromocenter Formation and Correct Gene Expression

During cellularization, a chromocenter is formed by centromeric heterochromatin, which remains condensed even in interphases [13]. At early stages of development, the chromatin is homogenous in appearance and the heterochromatin marker Heterochromatin protein 1 (HP1) is present throughout the nucleoplasm (Figure 2D). During cellularization, HP1 accumulates at the apical-located chromocenter, whereas reduced amounts of the protein are present basally in the nucleus (Figure 2D, [13]).

In *kuk* or *kur* embryos, the formation of a distinct chromocenter was impaired. In many nuclei, the strong apical HP1 staining was absent (Figure 2D). In only few nuclei, a very weakly stained chromocenter was detectable when compared to the wild-type situation at the same stage of development. Conspicuously, HP1 staining was still relatively homogeneously distributed throughout the nucleoplasm (Figure 2E).

For determining whether *kuk* and *kur* have an effect on gene expression, the genome-wide expression profiles in *kuk* and *kur* mutant embryos were compared to those of stage-matched wild-type embryos. We only selected genes with greater than 2-fold change in both genetic conditions. This revealed 96 genes with significant changes in gene expression (Tables S1 and S2). Interestingly, the set of downregulated genes ( $n = 88$ ) is strongly enriched for early zygotic genes ( $n = 23$ ), which

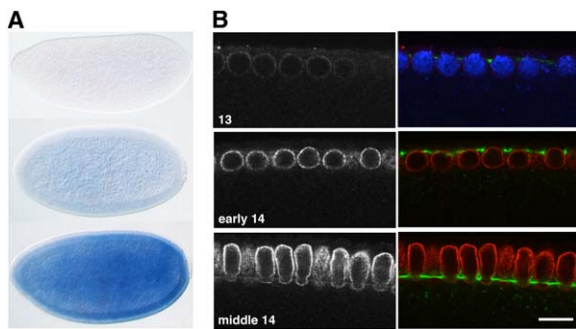


**Figure 3. Expression Pattern of *kuk***  
(A) In situ hybridization for *kuk* RNA. Embryos prior to pole-cell formation, in cycle 13, and in early cycle 14 (from top).  
(B) Wild-type embryos in stages as indicated and stained with Kuk antibody (white, red). The tip of the invaginating membrane is marked by Slam staining (green), and DNA is stained by Dapi (blue, only shown in the upper-right panel). The scale bar represents 10  $\mu$ m.

are induced during cellularization, e.g., *nullo*, *serendipity $\alpha$* , *slam*, *bottleneck*, or *frühstart*. In conclusion, in both *kuk* and *kur* embryos, the heterochromatin organization was affected and gene expression was altered. In the following, we will concentrate on the function of *kuk*, because we have not yet revealed the molecular nature of *kur*.

#### ***kuk* Encodes a Coiled-Coil Protein with Nuclear Localization Signal and CxxM Motif**

*kuk* encodes a protein of 570 amino acid (aa) residues. It contains a putative coiled-coil domain in the N-terminal half of the protein, a nuclear localization signal (NLS), and a C-terminal CxxM-motif, a putative site for farnesylation (Figure S2A). Kuk is so far the first described nuclear protein (see below), except for lamins, that contains a CxxM motif. Comparison with Kuk from other *Drosophila* species revealed an aa identity of 43% between Kuk from *D. melanogaster* and *D. virilis*. By Blast search, we found in the genomes of *Aedes aegyptii* and *Anopheles gambiae* two homologous, not-yet-annotated sequences (Figure S2B), which contained a conserved NLS together with a C-terminal CxxM motif but no obvious coiled-coil region. We did not find any homologous sequences in nonarthropod species.

In wild-type embryos, there is only weak expression of *kuk* during the first 13 division cycles (Figure 3A). In early interphase of cycle 14, *kuk* expression increased significantly. However, in pole cells, *kuk* expression remained constantly low during cellularization. Thus, increase of *kuk* transcription coincides with nuclear elongation.

#### **Localization of Kuk Protein in Embryos**

On a cellular level, Kuk appears to be exclusively localized to the nuclear envelope (Figure 3B). The electron-microscope analysis confirmed the nuclear-envelope localization and clearly showed that Kuk exclusively localizes to the nucleoplasmic side (Figures 4A–4C). As observed by confocal microscopy, Kuk staining only partially overlapped with nuclear pores visualized by antibodies against the nuclear-pore marker Nup50 (Figure 4D). The electron-microscope analysis,

however, revealed that Kuk staining is not present at nuclear pores (Figures 4A and 4C).

The antibody staining is specific because RNAi-injected embryos, embryos from *kuk* females (data not shown), and cultured *Drosophila* cells treated with *kuk* dsRNA (see below) lose the nuclear envelope staining for Kuk. Furthermore, the antibody detects recombinant Kuk protein expressed in reticulocyte lysate and *E. coli* as well as endogenous Kuk in extracts from wild-type embryos but not *kuk*-deficient embryos in western blots (Figure S1C).

The immunohistological localization of Kuk was confirmed by biochemical fractionation of embryos. Kuk and Dm0, the *Drosophila* lamin B, were both highly enriched in the nuclear fraction together other nuclear proteins (Figure 5A). Kuk and Dm0 were both not extracted with high-salt but with high-pH buffer (carbonate), consistent with a membrane anchorage by a farnesyl residue. However, Dm0 required higher salt concentration than Kuk for extraction in the presence of 1% triton, suggesting that Kuk in this respect behaves differently than Dm0 and is not part of salt-stable complexes.

The increase of Kuk protein levels during cellularization is comparable to the increase of the mRNA expression levels. In early division cycles 10–13, Kuk staining was very weak (Figure 3E). It strongly increased in early interphase of cycle 14, when cellularization started (Figure 3E). Throughout cellularization, all somatic nuclei showed prominent Kuk staining. The pole cells showed a staining pattern distinct from that of somatic cells. During cycles 10–14, Kuk labeling was absent from the majority of the pole cells (Figure S3A). During mitosis, *kuk* localizes differently than Dm0 or the nuclear-pore marker antibody A141 (Figure S3B). The presence of Kuk in growing late-telophase or interphase nuclei may suggest a function in nuclear-membrane growth.

The localization of some [16] but not all [17] lamina proteins depends on Dm0. In *Dm0*-RNAi-treated cells, the localization of Kuk in the nuclear envelope was indistinguishable from that in control cells (Figures 5B and 5C). However, the localization of Otefin, a Dm0 interacting protein of the INM [18], was changed after *Dm0*-RNAi treatment, confirming the depletion of Dm0. No alterations in the Dm0 localization were observed in *kuk*-RNAi-treated cells. We conclude that Kuk targeting to the nucleoplasmic side of the nuclear envelope and its retention in this subcompartment is independent of Dm0.

#### ***Kuk* Overexpression in Embryos Results in Highly Lobulated Nuclei**

To study the activity of *kuk* in embryos, we injected *kuk* mRNA and fixed the embryos in blastoderm stage. The nuclei became strongly lobulated and wrinkled already early in cellularization (Figure 6B), whereas uninjected embryos possessed smooth, unruffled nuclear envelopes (Figure 6A). Similarly, embryos from transgenic flies with six copies of the *kuk* gene showed very ruffled and abnormally shaped nuclei (Figure 6F). Thus, overexpression of *kuk* resulted in a changed morphology that may be a consequence of extensive growth of the nuclear envelope. In later stages, during gastrulation, moderately wrinkled and lobulated nuclear shapes are typical for interphase nuclei (Figure 6D). In contrast, nuclei

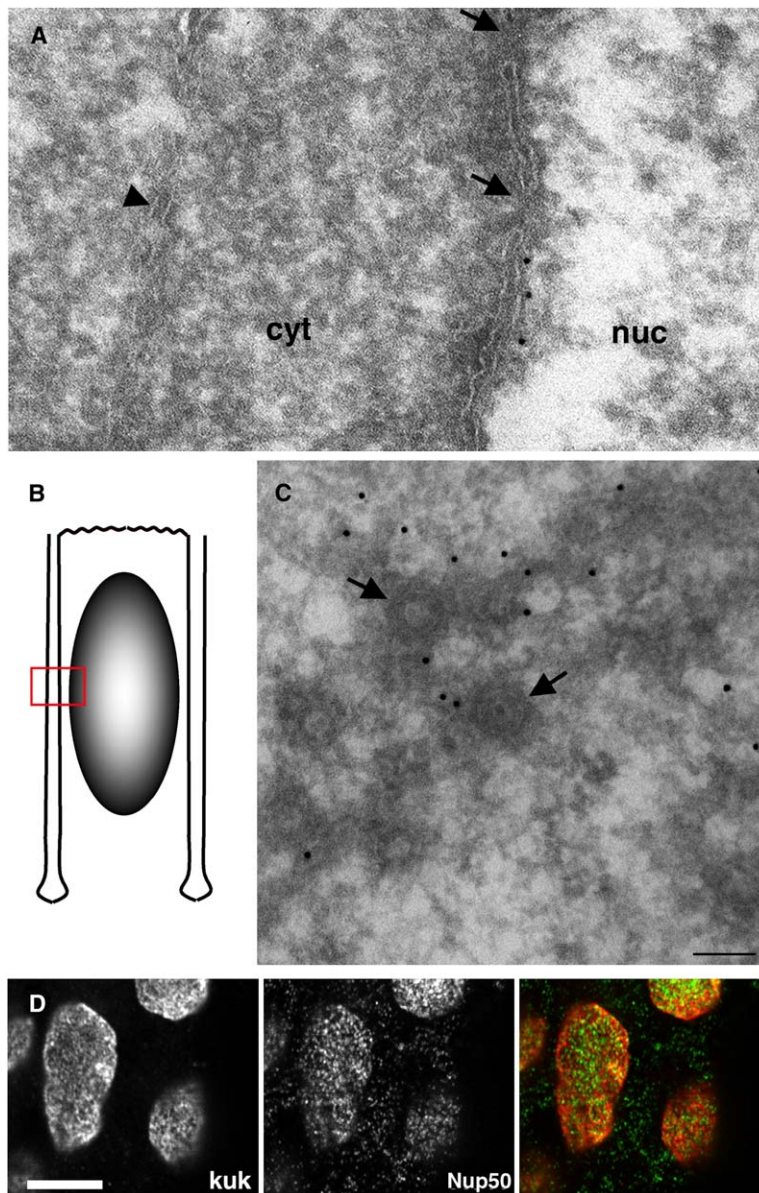


Figure 4. Localization of Kuk

(A) Immunoelectron microscopic analysis of embryonic nuclei reveals localization of Kuk at the inner nuclear membrane (black dots, 10 nm gold particles); arrows indicate nuclear pores, and arrowheads indicate cytoplasmic membranes; cyt denotes cytoplasm, and nuc denotes nucleoplasm.

(B) Schematic drawing of nucleus and invaginating membrane. Red rectangle indicates position of section shown in (A).

(C) Immunolabeling with Kuk antibodies in a tangential section of a nucleus (10 nm gold particles). Several nuclear pores (arrows) are visible (scale bar represents 100 nm). Kuk does not localize to nuclear pores.

(D) Amnioserosa nuclei from late embryos double-labeled with Kuk (red) and Nup50 (green) antibodies. The scale bar represents 5  $\mu\text{m}$ .

in *kuk*-RNAi-treated embryos or embryos from *kuk* females were round and unruffled (Figure 6E). In conclusion, we observed a correlation of the expression of *kuk* and ruffled nuclear morphology.

To test whether *kur* functions independently of *kuk*, we injected *kuk* dsRNA into *kur* embryos. However, there was no visible alteration from the *kuk* phenotype in those RNAi-treated embryos. When we overexpressed *kuk* mRNA in *kur* embryos, a comparable phenotype to overexpression in wild-type embryos was observed (Figure 6C). This indicates that *kur* may function either upstream or independently of *kuk*.

#### ***kuk* Affects Nuclear Morphology in *Xenopus* Cells**

Kuk localizes exclusively to the nuclear envelope when expressed in *Xenopus* A6 cells (Figures 6G–6J). The transfected nuclei became significantly larger (nuclear perimeter is almost doubled,  $p < 0.001$ , Figure 7G), and the nuclear envelope was more folded, containing

deep indentations, compared to nuclei of untransfected control cells (Figures 6G–6J). Costaining for Kuk and XLam B2 revealed strict colocalization of Kuk with lamin B2 over the entire nuclear envelope, including additional intranuclear structures (Figures 6G and 6H). The costaining with Concanavalin A indicates that these intranuclear structures contain membranes and may represent deep indentations of the nuclear envelope (Figures 6I and 6J; [19–21]).

A drastic nuclear-surface enlargement accompanied by the presence of membranous structures inside the nucleus (Figure 6K) was observed by transmission electron microscopy. These additional structures within the nucleus (Figure 6L, asterisks) consisted of double membranes that enclose membrane profiles and ribosomes, structures typical for the cytoplasmic compartment. There were no obvious nuclear pores visible in these intranuclear membranes. Conclusively, the ectopic expression of *kuk* in A6 cells caused primarily nuclear

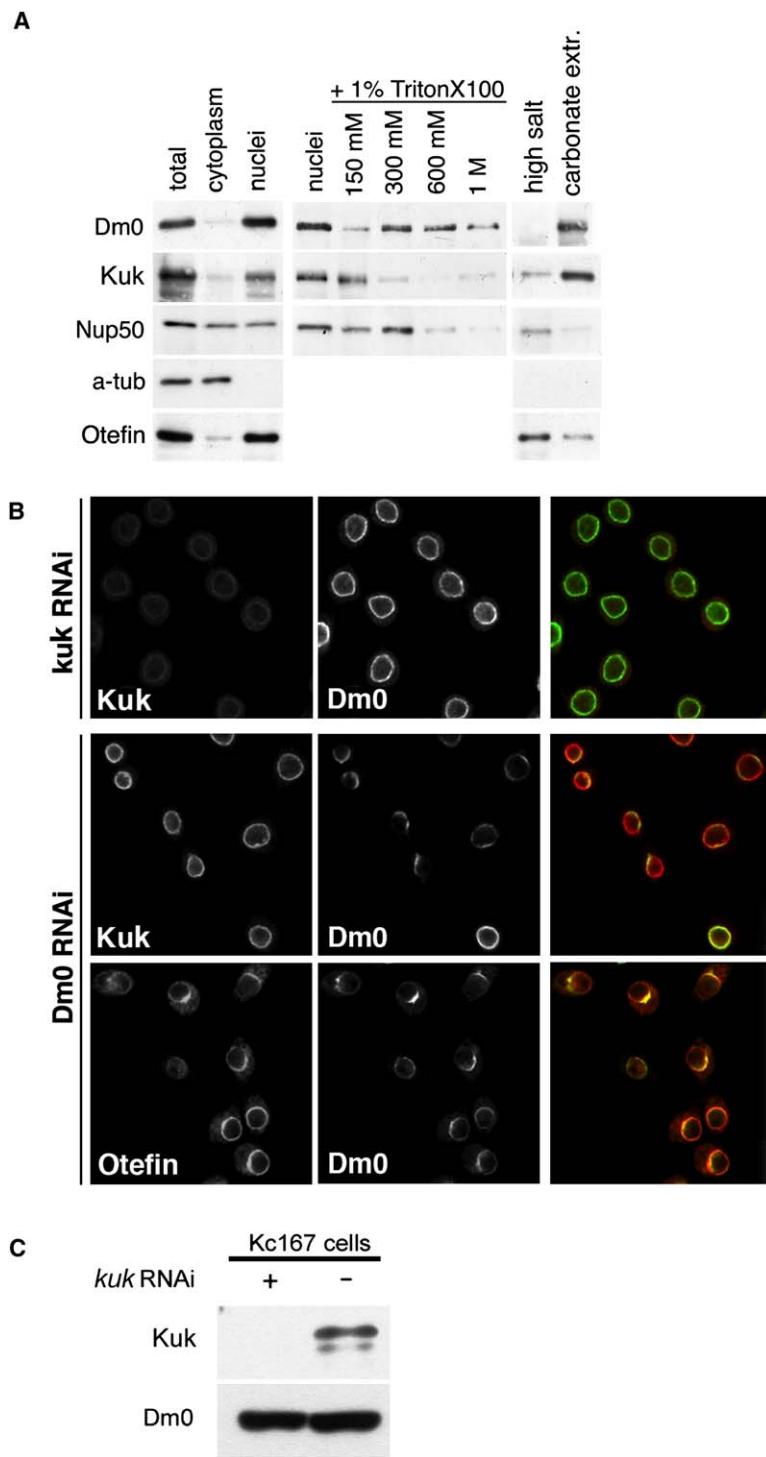


**Figure 5. Kugelkern and LaminDm0 Have Independent Functions**

(A) Subcellular fractionation and sequential extraction with increasing concentrations of NaCl ( $\alpha$ -tub,  $\alpha$ - tubulin).

(B) Downregulation of *kuk* and *Dm0*. *Drosophila* Kc167 cells treated with *kuk* or *Dm0* dsRNA were stained for Kuk (white, red), Dm0 (white, green), and Otefin (white, red) as indicated.

(C) Extracts of Kc167 cells treated with *kuk* dsRNA analyzed by western blot with indicated antibodies.

growth that manifests in an extended nuclear surface together with an altered morphology of the nucleus. The activity of *kuk* in *Xenopus* cells suggests that *kuk* employs a conserved mechanism to control nuclear morphology.

**All Three Motifs Are Required for Kuk Activity**

To characterize the function of the three different structural components of Kuk in detail, we expressed a series of truncated proteins and a nonfarnesylatable mutant

version of Kuk (KukSxxM, Figure 7F). Kuk-SxxM and the deletion protein C489 were distributed evenly throughout the nucleoplasm and did not affect nuclear size and shape (Figure 7A). Deletion proteins missing the NLS were homogeneously localized in the cell (Figure 7C, mutant C328). Deletion proteins lacking N-terminal aa residues (N136, N275) were located at the nuclear envelope. However, alterations in nuclear morphology were only present in cells expressing a mutant that contained the coiled-coil region (N136, Figures 7D and 7G).

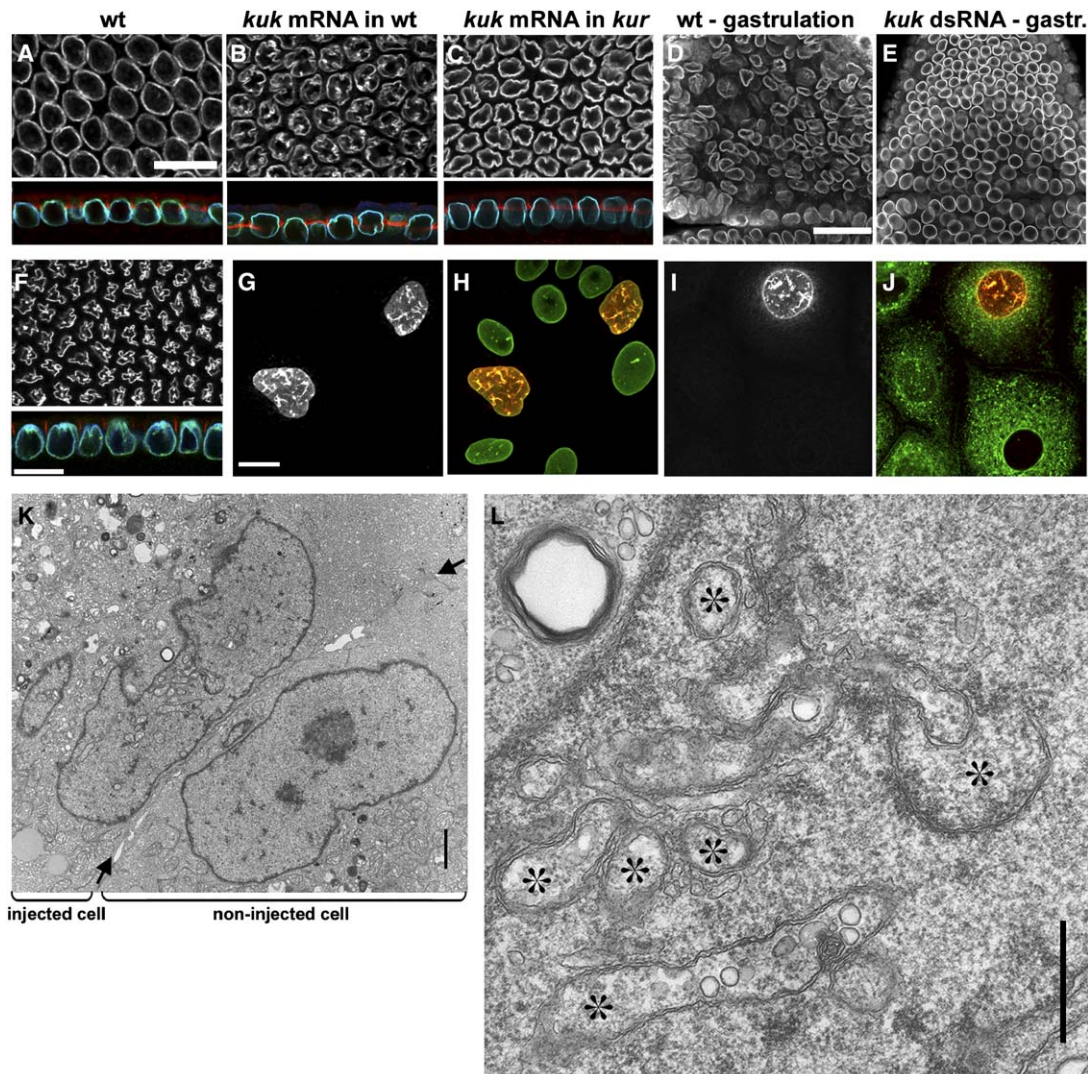


Figure 6. *kugelkern* Induces Nuclear-Membrane Growth

(A–C) Tangential (upper panels) and longitudinal (lower panels) section of embryos ([A], wild-type; [B], wild-type injected with *kuk* mRNA; [C], *kur* embryos injected with *kuk* mRNA) early in cellularization, stained for Kuk (white, green), Dm0 (blue), and f-actin (red). (D and E) Anterior region of a wild-type and *kuk*-RNAi-treated embryo during gastrulation, stained with Dm0. The scale bar (D and E) represents 25  $\mu$ m. (F) Embryo with six copies of *kuk* early in cellularization, stained for Kuk (white, green), Dm0 (blue), and Dlg (red). (G–J) Kuk expression in *Xenopus* A6 cells. Cells transfected with full-length *kuk* construct were stained for Kuk (white, red), XLam B2 ([G], green), and membranes (ConcanavalinA, [J], green). The scale bar represents 10  $\mu$ m. (K and L) Intranuclear structures analyzed by transmission electron microscopy. (K) Ultrathin section of a *kuk*-injected and an uninjected control cell. The cell borders are indicated by arrows. The scale bar represents 1  $\mu$ m. (L) Higher magnification of the *kuk*-expressing nucleus in (G). The lumina of the tubular structures (asterisk) contain vesicles and ribosomes. The scale bar represents 0.5  $\mu$ m.

Other C-terminal (C153) or N-terminal (N437) deletion mutants lacking most of the molecule were localized in the nucleoplasm as well as the cytoplasm and did not influence the nuclear morphology (Figure 7F). Thus, all three motifs together are required for the morphogenetic activity of Kuk.

## Discussion

The morphology of the nuclei changes dramatically during cellularization. We confirmed [14] that nuclear size indeed increases independently of MT. Thus, nuclear shape change and nuclear growth may be two separate

processes, regulated independently. We favor the model that nuclear size increase is a nuclear-autonomous process and the growing nuclei are directed passively by the MT basket into an ellipsoidal shape.

What may be the function of Kuk during cellularization? Although the nuclear size increase is impaired in *kuk*- and *kur*-depleted embryos, no other defects, e.g., concerning plasma-membrane invagination or the actin cytoskeleton, are observed. Consistent with the hypothesis that in *kuk* embryos a nuclear-intrinsic process is affected, we find that Kuk exclusively localizes to the INM. Because *kuk* and *kur* embryos show divergent phenotypes during gastrulation, we deduce that *kur* has during

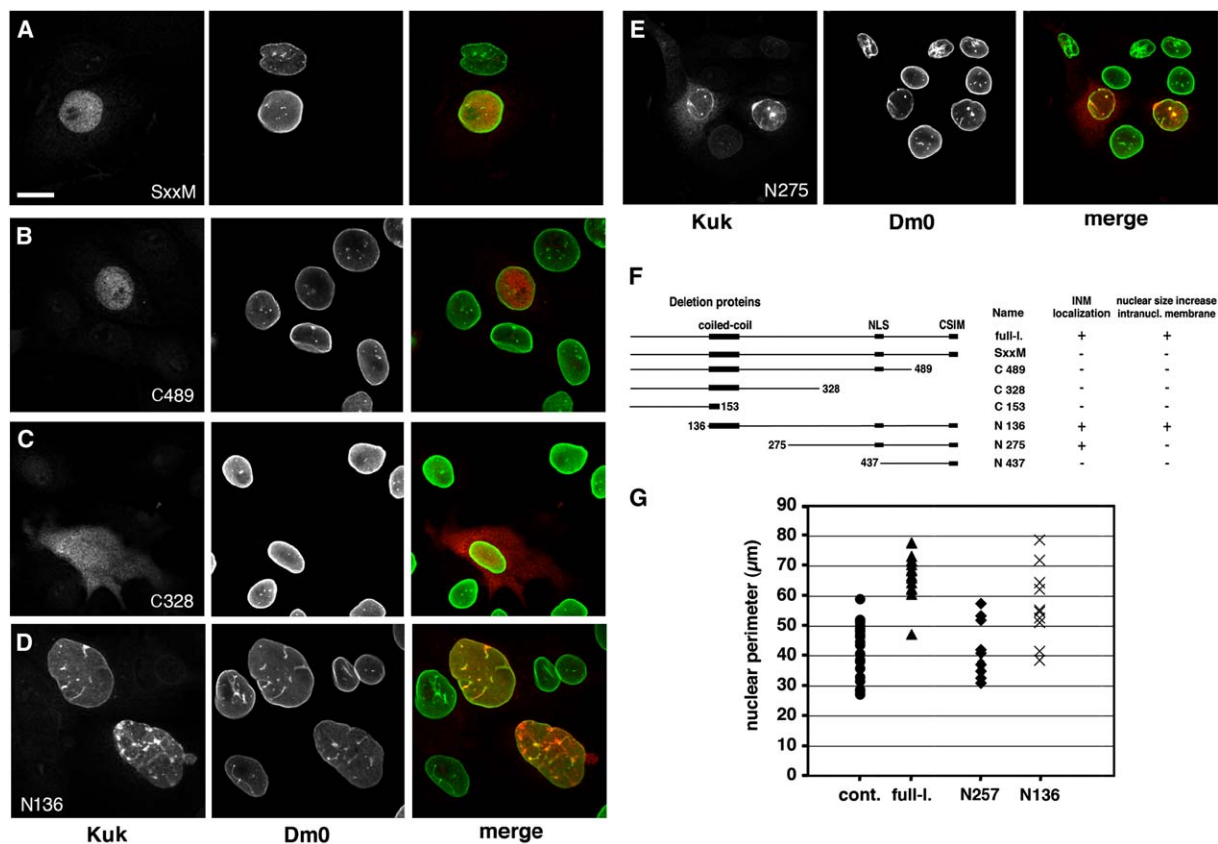


Figure 7. Deletion Mutants of *kuk* Expressed in *Xenopus* A6 Cells

(A–E) *Xenopus* A6 cells transfected with indicated *kuk* constructs and stained for Kuk (white, red) and XLam B2 (white, green).

(F) Schematic overview of the deletion constructs and summary of their activity. NLS denotes nuclear localization signal, and CSIM denotes farnesylation motif. (+) indicates localization of the expressed *kuk* construct to the nuclear envelope (INM) or whether larger nuclei with intranuclear structures were induced.

(G) Quantification of nuclear size by measuring the nuclear perimeter. Bidirectional Mann-Whitney test was applied to *kuk* full-length versus control cells (*kuk*: n = 16, control: n = 30; p < 0.001,  $U_A = 14$ , z = 5.2), N136 versus control cells (n = 10, p = 0.0005,  $U_A = 212$ , z = -3.46), and N275 versus control cells (n = 16, p = 0.992,  $U_A = 191$ , z = 0.01).

development a second, unknown function unrelated to the nuclear-elongation phenotype during cellularization. Insight into the function of *kur* has to await its molecular characterization.

*Kuk* shares some structural features, such as the nuclear localization signal (NLS), a coiled-coil domain, and the C-terminal CxxM-motif, with B type lamins. Interestingly, up to now, lamins were the only known nuclear proteins possessing a farnesyl moiety [22]. In addition to these similarities, *Kuk* exhibits properties distinct from that of lamins.

The overexpression of *Kuk* in embryos results in a nuclear morphology comparable to that found in gastrulating wild-type embryos. In contrast, *kuk*-depleted gastrulating embryos have smooth and unwrinkled nuclei typical for earlier stages. Thus, the overexpression phenotype of *kuk* may reflect precocious growth of the nuclear envelope. In *Xenopus* cells, *Kuk* induces additional membrane growth, the nuclei become larger, and the nuclear envelope is highly lobulated. By analyzing deletion constructs and a nonfarnesylated mutant of *Kuk*, we demonstrated that all three motifs, the coiled-coil region, the NLS, and the CxxM motif together are required for the morphogenetic activity of *Kuk*. These findings are

consistent with data from lamin-overexpression experiments in cultured mammalian, amphibian, or fish cells. In these studies, all lamin variants that contain an NLS together with the farnesylation motif show conspicuous overproliferation of NM [19, 22].

It seems unlikely that *kuk* takes part in the general phospholipid synthesis or membrane transport machinery, because in *kuk* embryos we see normal plasma-membrane invagination during cellularization. Most likely, *kuk* is part of a mechanism specific for nuclei. In principle, two different mechanisms are conceivable: (1), a catalytic function, where *Kuk* might induce membrane growth indirectly by activating effector components; and (2), a structural function, where *Kuk* might have a direct effect on the structure of the phospholipid bilayer. Insertion of farnesylated *Kuk* or Lamin B, acting like a wedge, would lead to a modification of the inner phospholipid layer by increasing the lateral packing stress of the membrane. This deformation in turn could induce incorporation of new phospholipids and thus allow expansion of the nuclear-membrane surface area. Consistent with this second model is our estimation of the number of *Kuk* molecules per nucleus ( $>10^4$ /nucleus, compared to  $>10^5$ /nucleus of Dm0). A structural model

is supported by studies of the activity of amphiphathic proteins on nuclear morphology. Incorporation of amphiphysin [23], CTP:phosphocholine cytidyl-transferase- $\alpha$  (CCT $\alpha$ , [20]), or Nup53 [24] into the nuclear envelope induces intranuclear, tubular membranes. Moreover, CCT $\alpha$  and amphiphysin have been shown to affect membrane curvature in vitro [20, 23]. How increased positive membrane curvature of the INM leads to the growth of the entire nuclear envelope remains to be elucidated.

Coincidental with nuclear elongation is the onset of zygotic transcription together with the rearrangement of the chromatin architecture. Strikingly, in both *kuk* and *kur* embryos, the reorganization of the chromatin is affected. Because this difference in chromatin organization is found independently in *kuk* as well as in *kur* embryos, we conclude that this phenotype might be related to the reduced nuclear size or nuclear surface area in both mutants. HP1 is known to be associated with heterochromatin and to influence gene expression [13, 25]. It can also interact with the inner nuclear-membrane protein LBR (Lamin B receptor, [26]) and thus may represent an adaptor between nuclear lamina and chromatin [27]. Indeed, we found that gene expression is altered in *kuk* and *kur* embryos. Convincingly, a specific set of genes are downregulated in both *kuk* and *kur* embryos in parallel, which suggests a connection between reduced nuclear surface area and transcriptional regulation. It is clear, however, that the nuclear elongation is not essential but only contributes to full onset of gene expression during cellularization.

Mutations in proteins of the lamina cause a wide range of human diseases, collectively called laminopathies [5], e.g., Hutchinson-Gilford progeria syndrome (HGPS), where a dominant point mutation in the *LMNA* gene causes a premature-accelerated-aging-like disorder [28, 29]. In the HGPS cells, the *LMNA* precursor is not properly endoproteolytically processed, resulting in a mutated lamin A form that still contains a farnesylated C terminus. Cultured fibroblasts from HGPS patients show pronounced lobular nuclear shapes that correlate with defects in DNA replication and alteration in heterochromatin organization [5, 27]. Moreover, lymphocytes directly isolated from HGPS patients possess strikingly enlarged nuclei [28]. Cells depleted for the endoprotease FACE1/Zmpste24, the enzyme that cleaves the farnesylated C terminus of the premature lamin A, show similar dramatic changes in the nuclear morphology with extensively lobulated nuclei [9]. These similarities between the phenotypes of HGPS cells and cells overexpressing nuclear proteins, such as Kuk, B type lamins, or uncleaved lamin A, with a farnesylation motif might have implications for our understanding of the Hutchinson-Gilford progeria syndrome.

## Conclusions

The nuclear lamina controls the shape of the nucleus but also interacts with chromatin to regulate gene expression. Analyzing the control of nuclear shape in a simple genetic system will allow better investigation of the function of the lamina and its connection to the control of gene expression. One can speculate that overexpression of Kuk or Dm0 in adult flies may cause aging-like symptoms or even influences life span. The finding

that the structural motifs coiled-coil, NLS, and CxxM are characteristic for lamins as well as for nonlamins like Kuk can help to screen for more, functionally important nuclear envelope proteins.

## Experimental Procedures

### General Procedures

A comprehensive and detailed description of the methods and materials can be found in the [Supplemental Data](#).

*kuk* (CG5175) was identified in a project that was initiated to reveal the function of early zygotic genes and was performed in a collaboration of the laboratories of T.L and J.G. [30]. *fs(1)kur* maps to 2B17;3C6 and was isolated in a screen for blastoderm mutants (A.B., F.P. and J. G., unpublished data) from a collection of germline clone mutations (N.V., unpublished data) similar to the collection described by S. Luschnig [31]. Embryological procedures were applied according to standard protocols [32]. The microarray data were deposited to EBI MIAMExpress; see Accession Numbers.

### Histology

Embryos and *Xenopus* A6 and *Drosophila* Kc167 cells were fixed and stained according to standard procedures ([Supplemental Data](#), [19, 33]). In some cases, 0.5% Triton X-100 was added to the blocking solution to improve permeabilization.

### Drug Treatment

For nocodazole treatment, dechorionated embryos were incubated for 2.5 min in n-heptane to permeabilize the vitelline membrane, briefly rinsed in PBS + 0.1% Tween, incubated for 50 min at room temperature in PBS containing 50  $\mu$ g/ml nocodazole, and subsequently fixed with FA.

### Transfection and Microinjection of Cells

Cells were fixed and stained 24–48 hr after transfection. Microinjection together with a GFP construct and EM processing was performed according to [19, 33].

### Microscopy

Control embryos were always mounted on the same slide and processed in parallel. For comparing the relative fluorescence levels of HP1 staining along the apical-basal axis of the nuclei, 10 nuclei in each 5 *kur*- and *kuk*-RNAi-treated embryos were evaluated.

### Supplemental Data

Supplemental Data include Supplemental Experimental Procedures, three figures, and two tables and are available with this article online at: <http://www.current-biology.com/cgi/content/full/16/6/543/DC1/>.

### Acknowledgments

We thank D. Görlich, K. Kapp, F. Schnorrer, M. Sedorf, and the lab members for discussions, advice, and suggestions on the manuscript. We thank Y. Kussler-Schneider for technical assistance; K. Schild for microinjection and processing for EM; S. Panier, S. Lawo, and P. Gawlinski for antibody purification and characterization and initial fractionation experiments; S. Lawo for western in [Figure S3B](#); and D.T. and A.M. Brandt for support. We are grateful for materials, reagents, and fly stocks from D. Görlich, M. Hild, *Drosophila* Stock Center (Bloomington, Indiana), and Hybridoma bank (Iowa). N.V. was supported by the Boehringer Ingelheim Fonds, A.B. by a Forschungsstipendium of the Deutsche Forschungsgemeinschaft, and J.G. by the Emmy-Noether Programm of the Deutsche Forschungsgemeinschaft.

Received: December 20, 2005

Revised: January 21, 2006

Accepted: January 24, 2006

Published online: February 2, 2006

## References

- Haithcock, E., Dayani, Y., Neufeld, E., Zahand, A.J., Feinstein, N., Mattout, A., Gruenbaum, Y., and Liu, J. (2005). Age-related changes of nuclear architecture in *Caenorhabditis elegans*. *Proc. Natl. Acad. Sci. USA* *102*, 16690–16695.
- Goldman, R.D., Shumaker, D.K., Erdos, M.R., Eriksson, M., Goldman, A.E., Gordon, L.B., Gruenbaum, Y., Khuon, S., Mendez, M., Varga, R., et al. (2004). Accumulation of mutant lamin A causes progressive changes in nuclear architecture in Hutchinson-Gilford progeria syndrome. *Proc. Natl. Acad. Sci. USA* *101*, 8963–8968.
- Gisselsson, D., Bjork, J., Hoglund, M., Mertens, F., Dal Cin, P., Akerman, M., and Mandahl, N. (2001). Abnormal nuclear shape in solid tumors reflects mitotic instability. *Am. J. Pathol.* *158*, 199–206.
- Gruenbaum, Y., Goldman, R.D., Meyuhos, R., Mills, E., Margalit, A., Fridkin, A., Dayani, Y., Prokocimer, M., and Enosh, A. (2003). The nuclear lamina and its functions in the nucleus. *Int. Rev. Cytol.* *226*, 1–62.
- Gruenbaum, Y., Margalit, A., Goldman, R.D., Shumaker, D.K., and Wilson, K.L. (2005). The nuclear lamina comes of age. *Nat. Rev. Mol. Cell Biol.* *6*, 21–31.
- Lenz-Böhme, B., Wismar, J., Fuchs, S., Reifegerste, R., Buchner, E., Betz, H., and Schmitt, B. (1997). Insertional mutation of the *Drosophila* nuclear lamin Dm0 gene results in defective nuclear envelopes, clustering of nuclear pore complexes, and accumulation of annulate lamellae. *J. Cell Biol.* *137*, 1001–1016.
- Cohen, M., Lee, K.K., Wilson, K.L., and Gruenbaum, Y. (2001). Transcriptional repression, apoptosis, human disease and the functional evolution of the nuclear lamina. *Trends Biochem. Sci.* *26*, 41–47.
- Krohne, G. (1998). Lamin assembly in vivo. *Subcell. Biochem.* *1*, 563–586.
- Varela, I., Cadinanos, J., Pendas, A.M., Gutierrez-Fernandez, A., Folgueras, A.R., Sanchez, L.M., Zhou, Z., Rodriguez, F.J., Stewart, C.L., Vega, J.A., et al. (2005). Accelerated ageing in mice deficient in Zmpste24 protease is linked to p53 signalling activation. *Nature* *437*, 564–568.
- Foe, V.E., Odell, G., and Edgar, B. (1993). Mitosis and morphogenesis in the *Drosophila* embryo: point and counterpoint. In *The Development of Drosophila melanogaster*, M. Bate and A. Martinez Arias, eds. (New York: Cold Spring Harbor Laboratory Press), pp. 149–300.
- Schejter, E.D., and Wieschaus, E. (1993). Functional elements of the cytoskeleton in the early *Drosophila* embryo. *Annu. Rev. Cell Biol.* *9*, 67–99.
- Sonnenblick, B.P. (1950). The early embryology of *Drosophila melanogaster*. In *Biology of Drosophila*. M. Demerec, ed. (New York: Wiley and Son), pp. 62–167.
- Kellum, R., Raff, J.W., and Alberts, B.M. (1995). Heterochromatin protein 1 distribution during development and during the cell cycle in *Drosophila* embryos. *J. Cell Sci.* *108*, 1407–1418.
- Edgar, B.A., Odell, G.M., and Schubiger, G. (1987). Cytoarchitecture and the patterning of fushi tarazu expression in the *Drosophila* blastoderm. *Genes Dev.* *1*, 1226–1237.
- Irvine, K.D., and Wieschaus, E. (1994). Cell intercalation during *Drosophila* germband extension and its regulation by pair-rule segmentation genes. *Development* *120*, 827–841.
- Wagner, N., Schmitt, J., and Krohne, G. (2004a). Two novel LEM-domain proteins are splice products of the annotated *Drosophila melanogaster* gene CG9424 (Bocksbeutel). *Eur. J. Cell Biol.* *82*, 605–616.
- Wagner, N., Weber, D., Seitz, S., and Krohne, G. (2004b). The lamin B receptor of *Drosophila melanogaster*. *J. Cell Sci.* *117*, 2015–2028.
- Goldberg, M., Lu, H., Stuurman, N., Ashery-Padan, R., Weiss, A.M., Yu, J., Bhattacharyya, D., Fisher, P.A., Gruenbaum, Y., and Wolfner, M.F. (1998). Interactions among *Drosophila* nuclear envelope proteins lamin, otefin, and YA. *Mol. Cell. Biol.* *18*, 4315–4323.
- Prüfert, K., Vogel, A., and Krohne, G. (2004). The lamin CxxM motif promotes nuclear membrane growth. *J. Cell Sci.* *117*, 6105–6116.
- Lagace, T.A., and Ridgway, N.D. (2005). The rate-limiting enzyme in phosphatidylcholine synthesis regulates proliferation of the nucleoplasmic reticulum. *Mol. Biol. Cell* *16*, 1120–1130.
- Fricke, M., Hollinshead, M., White, N., and Vaux, D. (1997). Interphase nuclei of many mammalian cell types contain deep, dynamic, tubular membrane-bound invaginations of the nuclear envelope. *J. Cell Biol.* *136*, 531–544.
- Ralle, T., Grund, C., Franke, W.W., and Stick, R. (2004). Intracellular membrane structure formations by CaaX-containing nuclear proteins. *J. Cell Sci.* *117*, 6095–6104.
- Peter, B.J., Kent, H.M., Mills, I.G., Vallis, Y., Butler, P.J., Evans, P.R., and McMahon, H.T. (2004). BAR domains as sensors of membrane curvature: the amphiphysin BAR structure. *Science* *303*, 495–499.
- Marelli, M., Lusk, C.P., Chan, H., Aitchison, J.D., and Wozniak, R.W. (2001). A link between the synthesis of nucleoporins and the biogenesis of the nuclear envelope. *J. Cell Biol.* *153*, 709–724.
- Piacentini, L., Fanti, L., Berloco, M., Perrini, B., and Pimpinelli, S.J. (2003). Heterochromatin protein 1 (HP1) is associated with induced gene expression in *Drosophila* euchromatin. *J. Cell Biol.* *161*, 671–672.
- Ye, Q., Callebaut, I., Pezhman, A., Courvalin, J.C., and Worman, H.J. (1997). Domain-specific interactions of human HP1-type chromodomain proteins and inner nuclear membrane protein LBR. *J. Biol. Chem.* *272*, 14983–14989.
- Scaffidi, P., and Misteli, T. (2005). Reversal of the cellular phenotype in the premature aging disease Hutchinson-Gilford progeria syndrome. *Nat. Med.* *11*, 440–445.
- De Sandre-Giovannoli, A., Bernard, R., Cau, P., Navarro, C., Amiel, J., Boccaccio, I., Lyonnet, S., Stewart, C.L., Munnich, A., Le Merrer, M., et al. (2003). Lamin A truncation in Hutchinson-Gilford progeria. *Science* *300*, 2055.
- Eriksson, M., Brown, W.T., Gordon, L.B., Glynn, M.W., Singer, J., Scott, L., Erdos, M.R., Robbins, C.M., Moses, T.Y., Berglund, P., et al. (2003). Recurrent de novo point mutations in lamin A cause Hutchinson-Gilford progeria syndrome. *Nature* *423*, 293–298.
- Pilot, F., Philippe, J.M., Lemmers, C., Chauvin, J.P., and Lecuit, T. (2006). Developmental control of nuclear morphogenesis and anchoring by charleston, identified in a functional genomic screen of *Drosophila* cellularisation. *Development* *133*, 711–723.
- Luschnig, S., Moussian, B., Krauss, J., Desjeux, I., Perkovic, J., and Nusslein-Volhard, C. (2004). An F1 genetic screen for maternal-effect mutations affecting embryonic pattern formation in *Drosophila melanogaster*. *Genetics* *167*, 325–342.
- Roberts, D.B. (1998). *Drosophila*, A Practical Approach. (Oxford, UK: Oxford University Press).
- Prüfert, K., Alsheimer, M., Benavente, R., and Krohne, G. (2005). The myristoylation site of meiotic lamin C2 promotes local nuclear membrane growth and the formation of intranuclear membranes in somatic cultured cells. *Eur. J. Cell Biol.* *84*, 637–646.

## Accession Numbers

The microarray data were deposited to EBI MIAMExpress with the accession numbers [E-TABM-75](#) (data) and [A-MEXP-314](#) (array design).

# Developmental Control of Nuclear Size and Shape by *kugelkern* and *kurzkern*

Anneli Brandt, Fani Papagiannouli, Nicole Wagner, Michaela Wilsch-Bräuninger, Martina Braun, Eileen E. Furlong, Silke Loserth, Christian Wenzl, Fanny Pilot, Nina Vogt, Thomas Lecuit, Georg Krohne, and Jörg Großhans

## Supplemental Experimental Procedures

### General Procedures

Genetic material and fly strains are described by FlyBase (<http://www.flybase.net>). Germline clones were produced with the Frt/ovoD system [S1]. The *Kuk* primary structure was analyzed by PSORT (<http://psort.nibb.ac.jp/form2.html>) and BLAST (<http://www.ncbi.nlm.nih.gov/BLAST/>).

### *kuk* Deletion and Rescue

For producing deletions of *kuk*, the *w*<sup>+</sup>-marked transposons EY07696 [excisions Df(3R)*kuk*24 and Df(3R)*kuk*15] and EY05076 [excision Df(3R)CG5169-2] were mobilized with transposase (Delta2-3 chromosome). White revertants were tested for complementation of the lethality of Df(3R)Exel6176 and of a lethal point mutation in CG5169 (S. Bartoszewski and J.G., unpublished data). The lethality due to loss of CG5169 was complemented with a genomic rescue transgene of CG5169 (P{CG5169<sup>+</sup>}). The nuclear-morphology phenotype of *kuk* was complemented by a maternal copy of the genomic transgene of *kuk* (P{kuk<sup>+</sup>}) but not by a zygotic wild-type allele. Breakpoints of deficiencies were determined by PCR with genomic DNA isolated from homozygous embryos or larvae. Deletions Df(3R)CG5169-2 and Df(3R)*kuk*15 do not complement the point mutation in CG5169, and their lethality is complemented by the CG5169 rescue transgene (P{CG5169<sup>+</sup>}). Deletion Df(3R)*kuk*24 complements the lethal point mutation in CG5169 and its distal breakpoint maps between *kuk* and CG5169. The proximal breakpoint of the deletion Df(3R)CG5169-2 is within the coding region of *kuk*. For the 6× *kuk* stock, insertions of the P{kuk<sup>+</sup>} on the X and III chromosomes were combined. The stock has a reduced viability and fertility (20% hatching rate).

DNA of the CG5169 locus (5.3 kb XhoI-XbaI fragment) or *kuk* locus (8.2 kb EcoRV-EcoRV fragment) was isolated from BACR01E04 (CHORI, Oakland, California), cloned into pBKS, transferred into pCasper4, and injected into embryos to produce transgenes.

### Immunization

*Kuk*-H6 protein expressed in *E. coli* from plasmid QE80-*kuk*H6 was purified by metal-chelate chromatography (lysis and washing in 50 mM Na-phosphate [pH 8], 300 mM NaCl, 25 mM imidazol, elution with 50 mM Na-phosphate [pH 8], 300 mM NaCl, 250 mM imidazol) followed by preparative SDS-PAGE. Rabbits and guinea pigs were immunized with the powderized gel slice mixed with Freud's adjuvans. IgG were purified by affinity chromatography with protein A Sepharose (Pharmacia). Antibodies specific for Slam (aa 1-681-His6) were raised in rabbits and guinea pigs, and antibodies specific for Nup50 (full-length-His6) were raised in rabbits (P. Gawlinski and J.G., unpublished data).

### Histology

In general, embryos were fixed with 4% formaldehyde in PBS/hep- tane for 20 min. For phalloidin/ $\alpha$ -tubulin staining, embryos were fixed with 8% formaldehyde for 50 min. In some cases, 0.5% Triton X-100 was added to the blocking solution to improve permeabilization. Consecutively, fixed embryos were stained in PBS + 0.2% Tween containing primary antibodies, fluorescent secondary antibodies (4  $\mu$ g/ml, Alexa, Molecular Probes), or DAPI (0.2  $\mu$ g/ml) and mounted in Aquapolymount (Polyscience). The following antibodies were used: *Kuk* (0.2  $\mu$ g/ml), Nup50 (0.2  $\mu$ g/ml), A414 (1:1000),  $\alpha$ -tubulin (Sigma, 0.2  $\mu$ g/ml), Slam (1:5000), HP1 (C1A9, 0.1  $\mu$ g/ml), and phalloidin coupled to Alexa dyes (6 nM, Molecular Probes). *kuk* transcripts were detected by RNA in situ hybridization with a digoxi-

genin-labeled probe (UTP-Digoxigenin, Roche) and digoxigenin antibody coupled with alkaline phosphatase (1:5000, Roche).

*Xenopus* A6 and *Drosophila* Kc167 cells were fixed, stained, and processed as described [S2, S3]. Primary antibodies were diluted in PBS containing 5% BSA as follows: *Kuk*, anti-HA, Otefin, *Xenopus* lamin B2 (X223), DmO (ADL84 and ADL195), fluorescent secondary antibodies (Texas Red, Cy2, Dianova, 1: 100), and Alexa-Concanavalin A (50  $\mu$ g/ml, Molecular Probes).

### Microinjection and Drug Treatment

Dechorionated embryos were injected posteriorly with 50–100  $\mu$ l of aqueous dsRNA (1  $\mu$ g/ $\mu$ l). After fixation of the embryos with 4% formaldehyde for 30 min, the vitelline membrane was removed manually.

### Microarray Analysis

Embryos were collected in intervals of less than 30 min and carefully staged by morphology. Only embryos of late stage 5, stage 6, and very early stage 7 (at the end of cellularization, before the pole cells reach the dorsal site) were included. Two independent embryo collections and hybridizations were performed for each mutant (wild-type embryos injected with *kuk* dsRNA, embryos from *kur* germline clones) and wild-type. Total RNA was extracted with RNeasy kits (Qiagen), amplified via the SMART method [S4], and Klenow labeled (Bioprime CGH kit, Invitrogen) with either Cy5- or Cy3-coupled dUTP (Amersham Biosciences). After purification via MinElute columns (Qiagen), 1  $\mu$ g of labeled mutant sample was hybridized together with 1  $\mu$ g of its respective wild-type control in 5× SSC, 0.1% SDS, 1% bovine serum albumin, and 25% formamide to INDAC (International *Drosophila* Array Consortium) 70-mer-oligo arrays. Dye swaps were performed to account for possible dye biases. The expression arrays consist of the *Drosophila* Genome Oligo Set, which contains 14,593 70 primer probes representing 13,664 genes and 17,899 transcripts. The arrays were scanned with Scanner Control Software software on a DNA Microarray scanner (Agilent Technologies). The raw data from the arrays were normalized with Tm4's print-tip LOWESS function [S5]. A one-class SAM was performed on four independent biological repeats for each time point. Genes with a *q* value < 0.05 and a signal change of *n* < 0.5 or *n* > 2 were considered to be differentially regulated.

### Real-Time PCR

cDNA was synthesized from 1  $\mu$ g total RNA isolated from staged embryos (late-cellularization, stage-6, early-stage-7, wild-type embryos injected with *kuk* dsRNA, and embryos from *kur* germline clones). PCR reactions contained 0.5  $\mu$ M of each primer (0.4  $\mu$ M in the case of RP49), DNA template, and Sybr-green PCR mix (Applied Biosystems). The amount of template was 3 ng, 300 pg, 30 pg, 3 pg for standards (wild-type cDNA) and 300 pg for the samples. The PCR products had lengths of about 300 bp. The standard curves were established in duplicates and the measurements in triplicates. The PCR was performed in a single 96-well plate in a ABI7500 machine (Applied Biosystems) according to the instructions of the manufacturer. Primer sequences were as follows: slam, JG241 GTGCAT CCAGCTGCAAGCAAT and JG242 CGGGCATTGGAAGTGGGTTA CA; CG14317, JG243 CCATTGGATAGCCGCTGGATT and JG244 GCTGCCACCGAGCTGGCAATT; CG7960, JG245 GAGCAGCC CAAGCCAGATT and JG246 GGATTGTGGTTGGCGTTGAAGT; CG15382, JG247 GCCGGCAGTTGCTGACAACA and JG248 GGAGT CCTCGTCTTGGCCTTGA; and RP49, rp49F GCTAAGCTGTCCGCAAAA and rp49R TCCGGTGGGCAGCATGTG.

Table S1. Microarray Data from *kuk* and *kur* Embryos

Gene Name	Symbol	Early Zygotic Gene	<i>kuk</i> (mean change)	<i>kur</i> (mean change)	q Value SAM Analysis
CG3048	Traf1		2.45	2.50	3.40
CG10479	CG10479		2.43	3.10	3.66
CG1641	sisA		2.21	2.73	3.50
CG5481	lea		2.12	2.97	3.74
CG9881	p16-ARC		2.11	2.28	3.30
CG3689	CG3689		2.07	2.11	3.85
CG11849	dan	x	2.05	2.47	4.21
CG5575	ken		2.02	2.39	3.02
CG9506	slam	x	0.11	0.11	3.37
CG15634	CG15634	x	0.22	0.21	2.07
CG15382	CG15382	x	0.22	0.19	0.00
CG12205	Bsg25A	x	0.23	0.18	2.42
CG7960	Bro	x	0.24	0.29	2.79
CG14317	CG14317	x	0.24	0.24	3.40
CG18269	CG18269	x	0.26	0.23	3.84
CG31695	scw	x	0.27	0.32	2.67
CG14426	nullo	x	0.27	0.36	3.3
CG13711	CG13711	x	0.29	0.33	3.20
CG8634	CG8634		0.30	0.25	3.23
CG1046	zen	x	0.30	0.30	0.00
CG7428	halo	x	0.32	0.31	2.84
CG14764	CG14764		0.32	0.31	4.98
CG13000	CG13000	x	0.33	0.39	2.09
CG3954	csw		0.33	0.33	3.28
CG17604	c(3)G		0.34	0.36	3.23
CG4911	CG4911		0.34	0.31	0.00
CG11490	CG11490		0.35	0.39	3.88
CG17082	CG17082		0.36	0.27	3.34
CG17962	frs	x	0.37	0.27	4.21
CG9571	CG9571	x	0.37	0.36	0.00
CG13713	CG13713	x	0.37	0.38	3.3
CG7015	CG7015		0.37	0.34	3.20
CG2944	gus		0.38	0.31	3.20
CG3679	CG3679		0.39	0.37	3.44
CG8808	Pdk		0.39	0.43	2.83
CG5978	CG5978		0.39	0.37	3.17
CG17678	cta		0.40	0.29	3.41
CG7979	CG7979		0.40	0.35	2.40
CG5560	CG5560	x	0.40	0.31	2.45
CG17957	sry-alpha	x	0.41	0.37	3.20
CG5203	CHIP		0.41	0.27	4.37
CG3273	sced		0.41	0.38	3.40
CG4965	twe		0.41	0.29	3.34
CG1962	CG1962		0.42	0.33	3.44
CG5263	smg		0.42	0.29	4.06
CG15737	CG15737		0.42	0.34	3.18
CG5704	CG5704		0.42	0.31	4.96
CG7037	Cbl		0.42	0.46	4.06
CG10393	amos	x	0.42	0.39	3.34
CG5053	CG5053	x	0.43	0.38	3.33
CG6357	CG6357		0.43	0.44	2.27
CG8679	CG8679		0.43	0.43	2.07
CG11660	CG11660		0.43	0.45	3.50
CG12399	Mad		0.43	0.37	2.07
CG40494	RhoGAP1A		0.43	0.50	2.56
CG18177	CG18177		0.43	0.45	2.80
CG12244	lic		0.44	0.42	2.81
CG3045	CG3045		0.44	0.35	2.45
CG12559	rl		0.44	0.34	3.77
CG17508	CG17508		0.44	0.33	3.21
CG31919	CG31919		0.45	0.38	2.72
CG17270	CG17270		0.45	0.38	3.21
CG10855	CG10855		0.45	0.43	3.81
CG32350	CG32350		0.45	0.27	3.77
CG4332	CG4332		0.46	0.44	2.59
CG9311	CG9311		0.46	0.45	3.83
CG7595	ck		0.46	0.49	0.00

(continued)

Table S1 (continued)

Gene Name	Symbol	Early Zygotic Gene	<i>kuk</i> (mean change)	<i>kur</i> (mean change)	q Value SAM Analysis
CG4656	CG4656	x	0.47	0.47	3.23
CG3709	CG3709		0.47	0.37	4.33
CR32028	CR32028		0.47	0.45	2.07
CG4993	PRL-1		0.47	0.46	2.97
CG3281	CG3281		0.47	0.46	1.76
CG17018	CG17018		0.47	0.32	3.77
CG8742	Gyc76C		0.47	0.42	3.02
CG17462	CG17462		0.48	0.43	3.84
CG40006	CG40006		0.48	0.45	2.34
CG7869	SuUR		0.48	0.50	3.27
CG14103	CG14103		0.48	0.42	2.01
CG9755	pum		0.48	0.49	4.24
CG7427	CG7427		0.48	0.40	2.70
CG18812	CG18812		0.48	0.41	2.65
CG3008	CG3008		0.48	0.45	3.62
CG6542	EDTP		0.48	0.43	3.84
CG12047	mud		0.48	0.44	2.72
CG10033	for		0.48	0.45	3.62
CG12891	CPTI		0.48	0.45	1.85
CG4063	ebi		0.48	0.45	3.40
CG3136	CG3136		0.49	0.45	2.64
CG32822	CG32822		0.49	0.40	4.41
CG8632	CG8632		0.49	0.49	2.73
CG9096	CycD		0.49	0.47	3.33
CG5608	CG5608		0.49	0.44	2.74
CG9493	Pez	x	0.50	0.40	2.76
CG11254	mael		0.50	0.38	2.85
CG9153	CG9153		0.50	0.47	2.72
CG10240	Cyp6a22		0.50	0.38	4.63

Microarray data of *kuk* and *kur* embryos. Genes with a peak of expression during cellularization as determined by microarray analysis ([S8] and [www.fruitfly.org/cgi-bin/ex/insitu.pl](http://www.fruitfly.org/cgi-bin/ex/insitu.pl)) and whole-mount in situ hybridization (C.W. and J.G., unpublished data) are marked with (x).

Table S2. Gene Expression Levels Measured by Real-Time PCR

Gene	Genotype	Slope <sup>a</sup>	Ct Value	Log (factor)	Factor (Reduction)
RP49	wild-type	-3.495	13.9		
	<i>kuk</i>		13.7		
	<i>kur</i>		13.5		
slam	wild-type	-3.589	20.8		
	<i>kuk</i>		24.1	0.9	8.3
	<i>kur</i>		25.5	1.3	20
CG14317	wild-type	-3.451	16.8		
	<i>kuk</i>		17.9	0.32	2.1
	<i>kur</i>		20.9	1.2	15
CG7960	wild-type	-3.412	17.3		
	<i>kuk</i>		19.3	0.59	3.9
	<i>kur</i>		21.3	1.2	15
CG15382	wild-type	-3.531	17.9		
	<i>kuk</i>		21.4	0.99	9.8
	<i>kur</i>		22.6	1.33	21

We analyzed the expression of four genes in wild-types and mutants by real-time PCR to verify the microarray analysis. Amplification of the product from the RNA sample occurred at least ten cycles later than from the cDNA sample (minus RT control). No amplification (Ct > 35) occurred with water as a template. The derivative of the melting curves of the products showed single peaks with T<sub>m</sub> = 82°C–85°C.

<sup>a</sup> Slope of the linear curve calculated by linear regression of the standard measurements.  $\log(\text{factor}) = (\text{Ct1} - \text{Ct2})/\text{slope}$ .

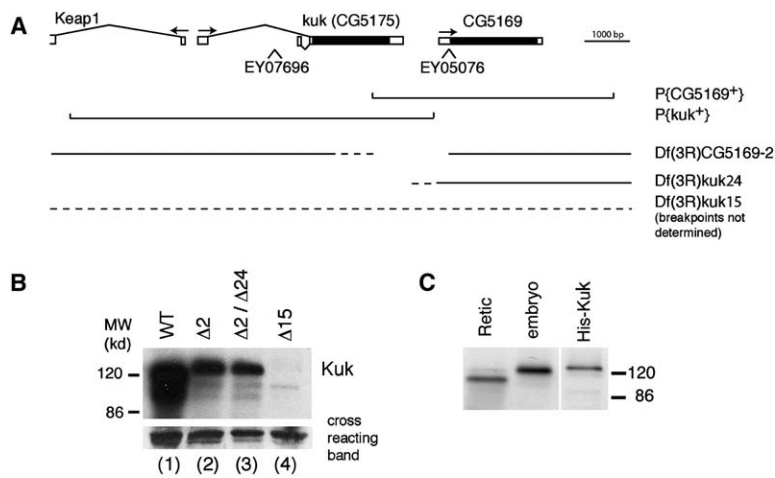


Figure S1. Genetic Characterization of the *kuk* Locus and Specificity of the Kuk Antibody

(A) Deletions of *kuk*. The genomic positions of *kuk* and its neighboring genes (annotation from Flybase), of two transposons (EY07696, EY05076), of a genomic rescue construct of the CG5169 gene (P{CG5169\*}), a genomic rescue construct of *kuk* (P{kuk\*}), and of three *kuk* deletions are indicated. Gaps indicate deficient regions, and dashed lines show uncertainties.

(B) Kuk protein expression in *kuk* deletions: Embryonic extracts (ten embryo equivalents, stage 9) with the following genotypes were analyzed by western blotting with Kuk antibody. Equal loading was controlled by a cross-reacting band. Genotypes of stocks were as follows: (1) WT, wild-type; (2) Δ2, P{CG5169\*}; Df(3R)CG5169-2; (3) Δ2/Δ24, P{CG5169\*}; Df(3R)CG5169-2; and (4) Δ15, P{CG5169\*}; Df(3R)kuk15/Df(3R)Exel6176. In the extracts from embryos with excision Df(3R)CG5169-2, a band with higher apparent molecular weight is detected, which may be due to an extended open reading frame of *kuk*. In fixed embryos from the stocks with the genotypes (2), (3), and (4), no localized Kuk antibody staining was observed.

(C) The antibody detects Kuk protein expressed in reticulocyte lysate and in *E. coli* as well as endogenous Kuk in embryonic extract. The Kuk band migrates at about 120 kd, probably representing a dimer. The Kuk band of reticulocyte lysate migrated slightly faster, possibly as a result of a differential modification.

#### Cell Culture, Transfection, and Microinjection of Cells

*Drosophila* Kc167 cells and *Xenopus* A6 cells were cultured according to standard procedures (Kc167 cells, 27°C; A6 cells, 27°C and 5% CO<sub>2</sub>). A6 cells (at 24 hr) were transfected with DNA by using FuGENE (Roche) according to the manufacturer's instructions. RNAi experiments in *Drosophila* Kc167 cells were performed as described [S6, S7]. Kc167 cells were either subjected to immunoblotting ( $5 \times 10^5$ ) or subjected to immunostaining ( $7.5 \times 10^5$  cells). For microinjection, cells were plated on CELLocate (Eppendorf) and injected with 40 ng/μl DNA for 0.2 s with 130 hPa pressure. A GFP-encoding plasmid was coinjected for identification. The position of the injected cells was determined prior embedding, sectioning, and EM processing.

#### Microscopy

Digital fluorescent images were taken with a confocal microscope (Leica) and processed with Photoshop (Adobe). Development of live embryos was recorded with an inverted microscope with differential interference contrast optics and a computer-controlled stage (Leica DMIRE2, Hamamatsu ORCA-ER, Openlab software, Improvi-

sion). Measurements were performed with ImageJ with the straight-line tool (nuclear length) or with the perimeter tool (nuclear perimeter) in a series of Kuk-stained embryos (Figure 1H). For Figures 1G, 2B, and 2C, Quicktime movies were converted into a series of pictures. For each graph, five nuclei of five different embryos were measured with the straight-line tool. Statistical analysis was performed with the VassarStats statistical computation program (<http://faculty.vassar.edu/lowry/VassarStats.html>). To compare the relative fluorescence levels of HP1 staining along the apical-basal axis of the nuclei, we fixed, stained, and mounted wild-type together with either *kuk* or *kur* embryos and photographed them with identical microscope settings. In ImageJ, ten nuclei were analyzed with the straight-line and plot-profile tools in  $n = 5$  embryos per group.

#### Electron Microscopy

For immunoelectron microscopy, blastoderm embryos were dechorionated and then fixed in 4% formaldehyde (paraformaldehyde dissolved in water), 0.05% glutaraldehyde in 0.1 M phosphate buffer, 1:1 with heptane overnight, washed with PBS + 0.01% Triton X-100, manually devitellinized, and fixed in 4% formaldehyde in 0.1 M

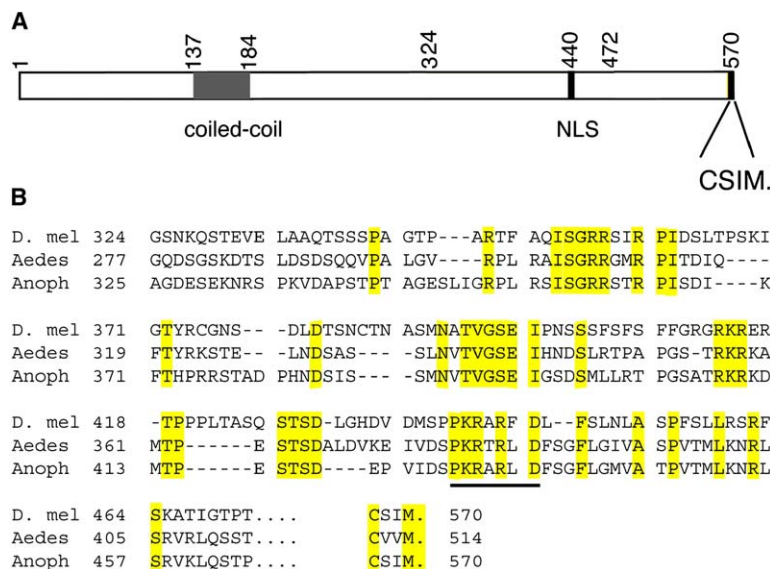


Figure S2. Structure and Conservation of *kuk*  
(A) Schematic of Kuk protein structure. Kuk contains a putative coiled-coil region, a putative nuclear localization signal (NLS), and a C-terminal CxxM motif indicating a potential farnesylation site.

(B) Partial sequence comparison of Kuk with two homologous sequences of *Aedes aegypti* and *Anopheles gambiae*. Identical amino acids are labeled in yellow; a bar marks the position of the conserved NLS. Note the conserved C termini.

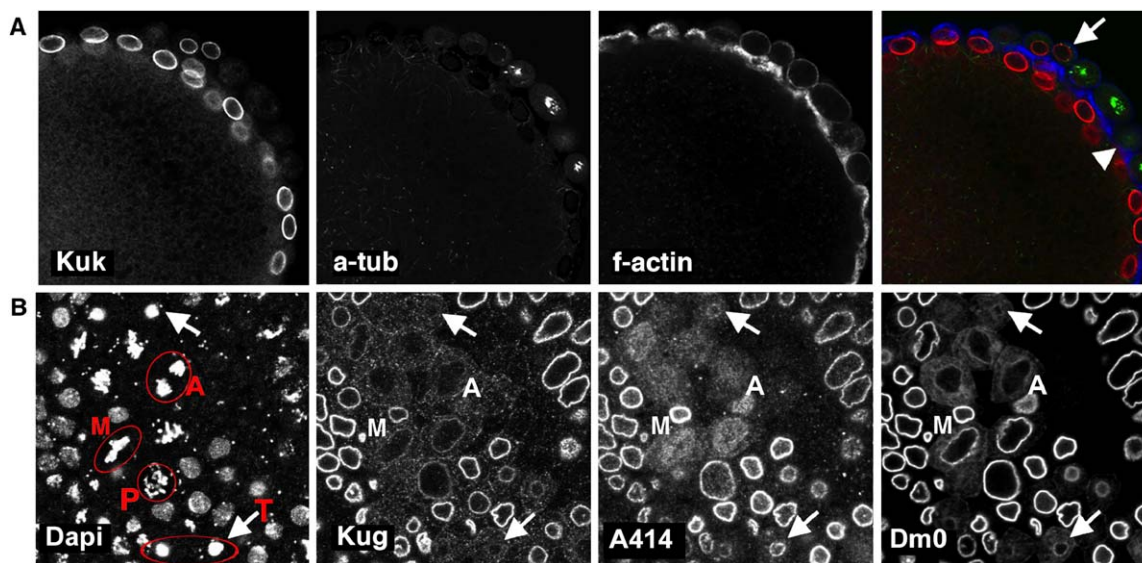


Figure S3. Differential Behavior of Kugelkern and LaminDm0 in Pole Cells and during Mitosis

(A) Pole cells in a cycle-12 embryo. Pairs of pole cells show staining for Kuk (red, arrow), whereas it is absent from most of the pole cells (arrowhead). Microtubule staining (green) marks mitotic cells. Staining for F-actin is shown in blue.

(B) Mitotic domain in anterior region of a gastrulating embryo with cells in different mitotic stages stained for Kuk, nuclear pores (Antibody 414), Dm0, and DNA. The following mitotic stages are indicated: prophase (P), metaphase (M), anaphase (A), and telophase (T). A telophase nucleus without Kuk staining is indicated by an arrow. During gastrulation, cells in different stages of the cell cycle can be found close to each other in the so-called mitotic domains. Kuk translocated from the NM to cytoplasm in early prophase, although at this point, Dm0 and the nuclear pore marker Ab414 were still present at the nuclear envelope. Kuk seems to be homogeneously distributed in the cytoplasm. Earliest Dm0 and Ab414 staining was visible in early telophase, when the nuclear envelope reforms. In contrast, the Kuk protein localized to the nuclear envelope slightly later in telophase. The first weak Kuk staining of the nuclear envelope was visible in relatively small nuclei, whereas the staining intensity was high in the larger mature interphase nuclei, which had an irregular morphology. The presence of Kuk in growing older telophase or interphase nuclei may suggest a function in nuclear-membrane growth.

phosphate buffer. Fixed embryos were incubated with 10% gelatine in 0.1 M phosphate buffer at 37°C for 15 min. Pieces of gelatine containing the embryos were infiltrated in 2.3 M sucrose in 0.1 M phosphate buffer. The samples were cryosectioned on a Leica UltracutUCT microtome with FCS cryochamber. The sections were retrieved with a 1:1 mixture of 2% methyl cellulose/2.3 M sucrose. After removal of the gelatine by incubation on PBS at 37°C, the sections were labeled with Kuk (2 µg/ml, from rabbit) primary antibody and detected with 10 nm gold-coupled Protein A (AZU, University of Utrecht, The Netherlands). The sections were contrasted with a mixture of 1.9% methyl cellulose/0.3% uranyl acetate for 10 min on ice. The samples were viewed in a Morgagni electron microscope (FEI Company).

Microinjected *Xenopus* A6 cells grown on CELLocate coverslips were fixed for 45 min with 2.5% glutaraldehyde (50 mM cacodylate [pH 7.2], 50 mM KCl, 2.5 mM MgCl<sub>2</sub>) at room temperature, subsequently fixed for 2 hr at 4°C with 2% osmium tetroxide buffered with 50 mM cacodylate (pH 7.2), washed with water, and incubated overnight at 4°C with 0.5% uranyl acetate. Cells were dehydrated, embedded in Epon812, and ultrathin sectioned. Sections were analyzed with a Zeiss EM10.

#### Molecular Genetics

SK-kuk (LD09231) was obtained from the Drosophila Genomics Research Center (Bloomington, Indiana). DNA encoding indicated fragments were amplified by PCR, cut by appropriate restriction enzymes, and cloned into the indicated vectors: QE-kuk-His6, as NcoI-BglIII into pQE80N60 (Görlich, Heidelberg); and CS-kuk, as EcoRI-XhoI and XhoI-XhoI from pSK-kuk into pCS2. C- and N-terminal deletion constructs kukΔN136 (aa 136–570), kukΔN194 (aa 194–570), kukΔN437 (aa 437–570), kukΔC153 (aa 1–153), kukΔC328 (aa 1–328), and kukΔC489 (aa 1–489) with an N-terminal 3×HA tag were synthesized as EcoRI-XbaI fragments by PCR and cloned into pCS2-HA. The point mutation C567S (codon 567 mutated to TCC) was introduced by inverse PCR with Pfu DNA polymerase. Synthetic

mRNA was synthesized with linearized templates and SP6 RNA-polymerase (Ambion). Double-stranded RNA for Dm0 was synthesized as described [S6]. DNA templates for the synthesis of kuk-specific dsRNA were amplified with a T7 promoter at their ends (LD09231: nt 766–1274). Respective dsRNA fragments were synthesized with T7 RNA polymerase (Ambion).

#### Biochemistry

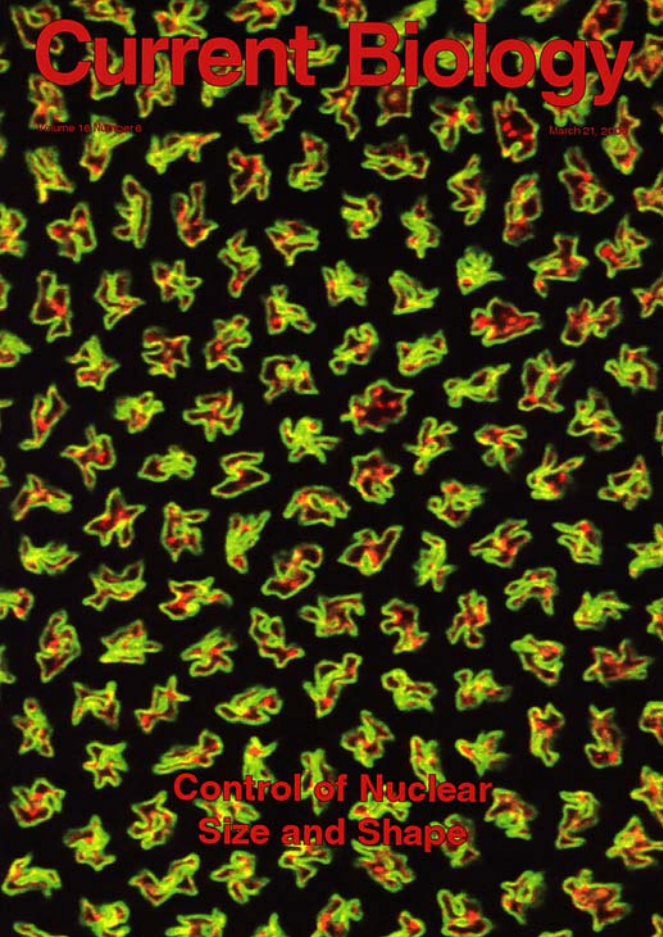
Proteins were analyzed by SDS polyacrylamid gel electrophoresis (SDS-PAGE) and western blotting according to standard protocols. The following antibody concentrations were used: α-tubulin (0.02 µg/ml, Sigma B152), otefin (1:5000), Dm0 (1:2000, polyclonal antibody), Nup50 (0.05 µg/ml), and Kuk (0.1 µg/ml). For sequential fractionation of nuclei, dechorionated embryos (100 mg) were homogenized in 1 ml lysis buffer (15 mM HEPES/KOH [pH 7.5], 10 mM KCl, 5 mM MgCl<sub>2</sub>, 1 mM DTT) with 0.35 M sucrose with ten strokes in a Dounce homogenizer. After centrifugation (10 min, 4k RPM) the pellet was suspended in 1 ml lysis puffer with 0.35 M sucrose, centrifuged (10 min, 4.6k RPM) through a cushion of 2 ml lysis puffer with 0.8 M sucrose, and washed twice in lysis buffer. The resulting nuclear fraction was sequentially extracted with 15 mM HEPES/KOH [pH 7.5], 1 mM DTT, 1% Triton X-100, and increasing concentrations of NaCl (150 mM, 300 mM, 600 mM, 1 M), or with high-salt buffer (15 mM HEPES/KOH [pH 7.5], 1 mM DTT, 1 M NaCl) and carbonate buffer (0.1 M Na-carbonate, pH 11). Equivalent of ten embryos per lane were analyzed by SDS-PAGE and western blotting.

#### Supplemental References

- S1. Chou, T.B., and Perrimon, N. (1996). The autosomal FLP-DFS technique for generating germline mosaics in *Drosophila melanogaster*. *Genetics* 44, 1673–1679.
- S2. Ralle, T., Grund, C., Franke, W.W., and Stick, R. (2004). Intracellular membrane structure formations by CaaX-containing nuclear proteins. *J. Cell Sci.* 117, 6095–6104.

- S3. Prüfert, K., Alsheimer, M., Benavente, R., and Krohne, G. (2005). The myristoylation site of meiotic lamin C2 promotes local nuclear membrane growth and the formation of intranuclear membranes in somatic cultured cells. *Eur. J. Cell Biol.* *84*, 637–646.
- S4. Petalidis, L., Bhattacharyya, S., Morris, G.A., Collins, V.P., Freeman, T.C., and Lyons, P.A. (2003). Global amplification of mRNA by template-switching PCR: linearity and application to microarray analysis. *Nucleic Acids Res.* *31*, e142.
- S5. Saeed, A.I., Sharov, V., White, J., Li, J., Liang, W., Bhagabati, N., Braisted, J., Klapa, M., Currier, T., Thiagarajan, M., et al. (2003). TM4: A free, open-source system for microarray data management and analysis. *Biotechniques* *34*, 374–378.
- S6. Prüfert, K., Vogel, A., and Krohne, G. (2004). The lamin CxxM motif promotes nuclear membrane growth. *J. Cell Sci.* *117*, 6105–6116.
- S7. Lagace, T.A., and Ridgway, N.D. (2005). The rate-limiting enzyme in phosphatidylcholine synthesis regulates proliferation of the nucleoplasmic reticulum. *Mol. Biol. Cell* *16*, 1120–1130.
- S8. Pilot, F., Philippe, J.M., Lemmers, C., Chauvin, J.P., and Lecuit, T. (2006). Developmental control of nuclear morphogenesis and anchoring by charleston, identified in a functional genomic screen of *Drosophila* cellularisation. *Development* *133*, 711–723.

# Current Biology

A dense field of individual cells, likely yeast, is shown against a black background. Each cell is brightly stained, with a green outline and a red nucleus. The cells exhibit various shapes and orientations, suggesting a population of cells in different stages of growth or division.

Volume 16 Number 6

March 21, 2008

**Control of Nuclear  
Size and Shape**